XXXVI Ibero-Latin American
Congress on Computational
Methods in Engineering
CILAMCE
Rio de Janeiro, 22-25 Nov 2015

TWO-FLUID MODEL FOR SLUG CAPTURE USING A LAGRANGIAN SCHEME

Marco Germano Conte, mg_conte@hotmail.com

Melissa Bianca Mendes, melissamendes@alunos.utfpr.edu.br

Fausto Arinos de A. Barbuto, fbarbuto@utfpr.edu.br

Rigoberto E. M. Morales, rmorales@utfpr.edu.br

Núcleo de Escoamentos Multifásicos - NUEM

Federal University of Technology – Paraná - UTFPR

Av. Sete de Setembro, 3165, Rebouças, CEP 80230-901, Curitiba – PR, Brasil

Abstract. *Two-phase slug flow in pipes occurs frequently in the petroleum and nuclear industries. By and large, slug flow differs from the other two-phase flow patterns due to its complexity. Slug flows are characterized by intermittent liquid slugs that fill the whole cross section of a pipe, followed by gas pockets called elongated gas bubbles. In recent decades, a few models for simulating such complex flows were developed, as the eulerian two-fluid model and drift flux, and the lagrangian slug tracking. The aim of this work is to present a detailed study on the numerical implementation of the hybrid model proposed by Fabien Renault and Nydal which is able to track down waves that arise in the gas-liquid interface and possible slugs generated by them. This model was developed from the two-fluid model equations in which the motion generated by the dynamic pressure of the gas on the slugs is decoupled from the slow movement of the liquid below the gas. The movement of the bubbles in the liquid is then modeled similarly to shallow-water equations. The solution of the equation set is achieved in two steps. The first step provides the pressure field and the gas flow through the numerical solution of the equations for the gas, using the finite difference method. The second step solves the adapted shallow-water equations analytically. The model was coded in object-oriented Intel Visual Fortran95. Simulations to analyze the ability of the code to generate slugs for some pairs of water-air superficial velocities at atmospheric pressure were carried out. The influence of the integration parameters (i.e. mesh size and time step) were analyzed and a criterion for the minimum grid length in order to maximize the number of slugs in the simulations for a given time step was proposed. The results, as the distribution of the slug length, bubble length, unit-cell frequency and mean slug frequency were compared to experimental data acquired at the NUEM/UTFPR labs to support slug initiation studies.*

Keywords: *Two-phase slug flow, slug capturing, slug initiation.*

1 INTRODUCTION

Two-phase slug flow is present in many industrial processes, such as the exploitation and transportation of hydrocarbon mixtures from oil wells. Slug flow is characterized by two distinct structures which repeat intermittently: a liquid slug with a large amount of momentum followed by a compressible gas bubble. This flow regime is the result of the growth and/or the interaction of small waves at the gas-liquid interface in horizontal or slightly inclined stratified flow (Lin and Hanratty, 1986; Fan et al., 1993), or due to liquid accumulation in regions where the pipeline inclination changes (Scott and Kouba, 1990; Zheng et al., 1994), e.g. terrain induced slugging (hilly terrain) and severe slugging.

Several authors have experimentally investigated the slug flow (Brill et al., 1981; Nydal et al., 1992; Van Hout et al., 2001; Woods et al., 2006). The liquid slug and bubble characteristics (length, holdup and velocity) and the frequency of these structures are usually the main focus of those studies. Experimental studies are of great worth to understand the dynamics and behaviour of any flow, and empirical correlations and mathematical models can be obtained from those studies. Yet, experimental works are restricted to pre-established conditions and the reproductions of actual scenarios are usually unrealistic due to the high costs involved.

Numerical analyses can be used as an alternative to study slug flows. The benefit of those analyses is that a general solution covering all the possible scenarios can be proposed. The first attempts to model slug flow are the so-called steady-state models in which the bubbles and slugs are evenly distributed in time and space (Dukler and Hubbard, 1975; Fernandes et al., 1983; Taitel and Barnea, 1990). Those models are easy to use and they predict the mean values of the important variables, such as the structures' lengths, the bubble translational velocity and the pressure drop.

The Eulerian formulation of the problem using a two-fluid model was developed in the 1980s for the nuclear industry based on authors such as Ishii (1975). The software OLGA (Bendiksen et al., 1991), a fairly used tool in the petroleum industry, was one of the first computational transient codes developed using the two-fluid model approach.

The Lagrangian formulation, based on the unit-cell concept introduced by Wallis (1969), was developed as an alternative. This concept considers a slug followed by a bubble as a unit cell. In this enunciation the grid follows those structures as they travel along the pipe. That is the case of the slug tracking methods (Barnea and Taitel, 1993; Zheng et al., 1994; Rodrigues et al., 2008).

Linear stability applied to the two-fluid model has been frequently used for theoretically determining whether a stratified smooth flow is either stable or unstable and whether slug flow is possible. The application of this theory to ideal flow where shear stresses are neglected leads to the inviscid Kelvin-Helmholtz (IKH) criterion (Taitel and Dukler, 1976). This analysis predicts the wave growth above the liquid-gas interface whenever the Bernoulli Effect overcomes the hydrostatic force. The linear stability analysis for viscous flows leads to the viscous Kelvin-Helmholtz (VKH) criterion (Lin and Hanratty, 1986; Barnea and Taitel, 1993).

Issa and Kempf (2003) solved a two-fluid model for a staggered grid and demonstrated its ability to capture perturbations on the interface of a stratified flow whenever the relative velocities of a system are between the IKH and VKH limits. Within those limits, the flow is mathematically well-posed and unstable. For velocities under VKH the flow is well-posed and stable whereas above IKH the flow is ill-posed with imaginary characteristics (Taitel and Dukler, 1976).

Renault (2007) also developed a methodology to simulate the region of transition between stratified and slug flow. A two-fluid model was solved by means of a hybrid schema. According to the author, this model showed good agreement with experiments and it is capable of simulating severe slugging flow.

Kjeldby et al. (2013) tested different slug initiation methods for severe slugging using a lagrangian formulation similar to Renault's. Several mesh sizes were tested. For fine grids, the Kelvin-Helmholtz instability triggered slug initiation whereas for larger grid sizes slugs were artificially introduced according to some transition criterion.

The present work uses the same model proposed by Renault (2007) translated into a computational code. The goals of this work are: to analyze such model, to show a complete methodology for slug initiation and to compare the results with experimental data acquired at the NUEM/UTFPR.

2 MATHEMATICAL MODEL

The two-fluid model applies the mass conservation and momentum balance equations to control volumes in the axial position for each phase individually. Figure 1 shows the transition from stratified to slug flow. The subscripts $_G$ and $_L$ denote gas and liquid, respectively; ρ is the phase density, g is the gravitational acceleration, U is the axial average velocity, p is the pressure and R is the phase volume fraction; J is the mixture velocity calculated by the sum of the superficial velocities of each phase (U_L^S ,U_L^G).

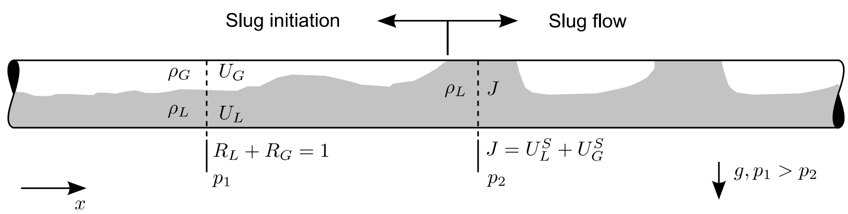

Figure 1. Representation of the transition between stratified and slug flow

The following assumptions are made: (1) one-dimensional flow; (2) no energy transfer; (3) no mass exchange; (4) constant cross-sectional area; (5) the surface tension effect is neglected; and (6) considering the pressure variation in the section occurs only due to the hydrostatic. Thus, the continuity equations for the liquid and gas become:

$$\frac{\partial}{\partial t}(\rho_L R_L) + \frac{\partial}{\partial x}(\rho_L R_L U_L) = 0 \tag{1}$$

$$\frac{\partial}{\partial t}(\rho_G R_G) + \frac{\partial}{\partial x}(\rho_G R_G U_G) = 0 \tag{2}$$

The momentum equations for each phase in horizontal flow are:

$$\frac{\partial}{\partial t}(\rho_L R_L U_L) + \frac{\partial}{\partial x}\left(\rho_L R_L U_L^2\right) = -\frac{\tau_L S_L}{A} + \frac{\tau_i S_i}{A} - R_L \frac{\partial p}{\partial x} - \rho_L g R_L \frac{\partial h_L}{\partial x} \tag{3}$$

$$\frac{\partial}{\partial t}\left(\rho_G R_G U_G\right)+\frac{\partial}{\partial x}\left(\rho_G R_G U_G^2\right)=-\frac{\tau_G S_G}{A}-\frac{\tau_i S_i}{A}-R_G\frac{\partial p}{\partial x}-\rho_G g R_G\frac{\partial h_L}{\partial x} \tag{4}$$

where τ is the shear stress, h_L is the liquid level, A is the cross-sectional area and S is the wetted perimeter. The subscript i denotes the liquid-gas interface.

Under the simplifications made by Renault (2007) and assuming: (1) incompressible liquid; (2) ideal gas; (3) gas momentum neglected compared to the liquid momentum and (4) gas locally incompressible in the resolution of the liquid momentum, the Eqs (1) and (3) can be rewritten as:

$$\frac{\partial}{\partial t}\left(R_L\right)+\frac{\partial}{\partial x}\left(R_L U_L\right)=0 \tag{5}$$

$$\frac{\partial}{\partial t}\left(R_L U_L\right)+\frac{\partial}{\partial x}\left(R_L U_L^2+\frac{1}{2}\kappa R_L^2\right)=\frac{R_L}{\rho_L}F \tag{6}$$

where F is the volumetric force:

$$F=-\frac{\tau_L S_L}{A_L}+\frac{\tau_G S_G}{A_G}+\tau_i S_i\left(\frac{1}{A_L}+\frac{1}{A_G}\right) \tag{7}$$

and

$$\kappa=\frac{\rho_L-\rho_G}{\rho_L}g\frac{A}{\frac{dA_L}{dh_L}}-\frac{1}{R_G}\frac{\rho_G}{\rho_L}\left(U_G-U_L\right)^2 \tag{8}$$

Equations (5) and (6) can be solved analytically through the solution of the Riemann problem (wave rarefaction and wave shock) as it will be shown below. Equations (5) and (6) can be written in matrix form as:

$$\left[M_A\right]\frac{\partial}{\partial t}\{\theta\}+\left[M_B\right]\frac{\partial}{\partial x}\{\theta\}=\{K\} \tag{9}$$

where θ is the vector of primitive variables $\theta=\{R_L,U_L\}$ and K is the source term. M_A and M_B are non-singular matrices whose elements are function of the flow variables and are given by:

$$M_A=\begin{bmatrix}1 & 0\\ U_L & R_L\end{bmatrix} \tag{10}$$

$$M_B=\begin{bmatrix}U_L & R_L\\ {U_L}^2+\kappa R_L & 2R_L U_L\end{bmatrix} \tag{11}$$

The characteristic value, λ, of the set of equations can be obtained by solving the following equation:

$$\det\left(\left[M_B\right]-\lambda\left[M_A\right]\right)=0 \tag{12}$$

Replacing M_A and M_B on Eq. (12), one finds:

$$\lambda^2 - 2U_L\lambda + U_L^{\ 2} - \kappa R_L = 0 \tag{13}$$

Eq. (13) has real characteristics provided that the parameter κ be greater than zero. Thus:

$$\kappa > 0 \rightarrow (U_G - U_L) < \left[(\rho_L R_G + \rho_G R_L) \frac{\rho_L - \rho_G}{\rho_L \rho_G} g \frac{A}{dA_L/dh_L} \right]^{0.5} \tag{14}$$

The simplified two-fluid model shown above is mathematically well-posed in the same region of the IKH criterion.

Closure Models

The liquid-wall and gas-wall shear stresses and the interfacial shear stress between the liquid and the gas are given by the following equations:

$$\tau_L = \frac{1}{2} f_L \rho_L U_L |U_L| \quad \tau_G = \frac{1}{2} f_G \rho_G U_G |U_G| \quad \tau_i = \frac{1}{2} f_i \rho_G (U_G - U_L)|U_G - U_L| \tag{15}$$

where f_L and f_G are the liquid-wall and gas-wall friction factors, respectively. For these variables, the Fanning friction factor was used for laminar flow whereas the Blasius equation was used for turbulent flow. They are calculated as function of Reynolds number and the hydraulic diameter as follows:

$$D_{hL} = 4\frac{A_L}{S_L} \quad D_{hG} = 4\frac{A_G}{S_G + S_i} \quad \mathrm{Re}_L = \frac{\rho_L D_{hL} U_L}{\mu_L} \quad \mathrm{Re}_G = \frac{\rho_G D_{hG} U_G}{\mu_G} \tag{16}$$

where Re is the Reynolds number, D_h is the hydraulic diameter and μ is the viscosity of each phase. For practical purposes, the biggest friction factor among the laminar and turbulent flows was used. A constant interfacial friction factor is used (f_i = 0.0142), as suggested by Cohen and Hanratty (1968).

The geometric parameters S, h_L and dA_L/dh_L are calculated as functions of ϕ as illustrated in Fig. 2, where D is the pipe diameter and ϕ is given by the relation derived by Biberg (2005):

$$\phi/2 = \pi R_L + \left(\frac{3\pi}{2}\right)^{1/3} \left[1 - 2R_L + R_L^{\ 1/3} - R_G^{\ 1/3}\right] \tag{17}$$

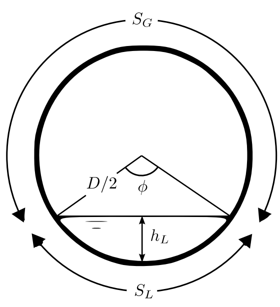

Figure 2. Stratified flow geometry

Table 1 shows a summary of the equations used for calculating the geometrical parameters and the friction factors.

Table 1. Friction factors and geometric parameters definition

Liquid-wall friction factor		$f_L = \begin{cases} 16\,\mathrm{Re}_L^{-1}, & if \ \mathrm{Re}_L \le 1000 \\ 0.079\,\mathrm{Re}_L^{-0.25}, & if \ \mathrm{Re}_L > 1000 \end{cases}$
Gas-wall friction factor		$f_G = \begin{cases} 16\,\mathrm{Re}_G^{-1}, & if \ \mathrm{Re}_G \le 1000 \\ 0.079\,\mathrm{Re}_G^{-0.25}, & if \ \mathrm{Re}_G > 1000 \end{cases}$
Interfacial friction factor (Cohen and Hanratty, 1968)		$f_i = 0.0142$
$\phi = \pi R_L + \left(\frac{3\pi}{2}\right)^{1/3}\left[1 - 2R_L + R_L^{\ 1/3} - R_G^{\ 1/3}\right]$		
$h_L = \frac{D}{2}\left(1 - \cos(\phi/2)\right)$	$A_L = \frac{D^2}{8}(\phi - \sin\phi)$	$\frac{dA_L}{dh_L} = D\sin(\phi/2)$
$S_L = D.\phi/2$	$S_G = D(\pi - \phi/2)$	$S_i = D\sin(\phi/2)$

The bubble-slug and slug-bubble border velocities can be calculated in two different ways: by using Bendiksen's (1984) correlation if a bubble nose is identified or through a liquid mass conservation equation when a slug front is found (see Fig. 3).

The bubble translational velocity is calculated using Bendiksen's correlation as:

$$U_B = \left(C_0 J + C_\infty\right) \tag{18}$$

where the coefficients C_0 and C_∞ are calculated as functions of the Reynolds and Froude numbers of the mixture, as shown in Tab. 2.

Table 2. Bubble translational velocity coefficients

	$Fr = \frac{J}{\sqrt{gD}}$	C_0	C_∞
$\mathrm{Re}_J > 1000$	> 3.5	1.2	0
	< 3.5	1.05	$0.54\sqrt{gD}$
$\mathrm{Re}_J < 1000$	-	2	$0.54\sqrt{gD}$

The coefficients used in this work are C_0 = 1.13 and C_∞ = −0.0104. Those coefficients were obtained experimentally.

As explained before, the slug translational velocity can be calculated from a liquid mass balance applied to a control volume moving with U_F in a region between the slug front and the bubble rear, as it can be seen in Fig. 3. In this work, slugs are non-aerated.

$$U_F = \frac{U_{LS} - R_{LB}U_{LB}}{1 - R_{LB}} \tag{19}$$

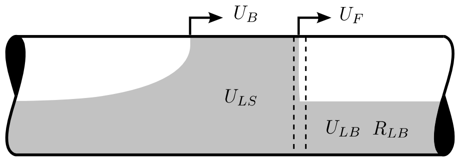

Figure 3. Slug front velocity calculation

The gas density is given by:

$$\rho_G(p) = \rho_{G,out} + \frac{\partial \rho_G}{\partial p}(p - p_{out}) \tag{20}$$

where $\partial\rho_G/\partial p$ is the gas compressibility, assumed as constant and calculated by the ideal gas law. p_{out} e $\rho_{G,out}$ are, respectively, the pressure and density of the gas in the pipe outlet and constitute the boundary conditions of the model.

3 NUMERICAL METHOD

The lagrangian solution proposed by Renault (2007) was used. In this method, the grid is free to move and follows the perturbations or waves that emerge from the liquid-gas interface and possible slugs.

The system of equations is solved in two steps. In the first step both the continuity and the momentum equations for the gas, Eqs. (2) and (4), are numerically solved using the finite difference method on a staggered grid. In the second step the continuity and momentum equations for the liquid, Eqs. (5) and (6), are analytically solved through the solution of the Riemann Problem (rarefaction and shock waves). The grid displacement is evaluated during this step.

Fig. 4 shows the computational grid. The pipe was discretized as cells that may represent either bubbles or slugs. Slugs are defined by a single cell whereas groups of more than one cell – henceforth called *sections* – define the stratified flow or bubble. The slugs store the mixture velocity (J), considered the same as the average liquid velocity ($J = U_{LS} \rightarrow R_L = 1$, for a non-aerated slug). The sections store the volume fraction (R_L), the average liquid velocity (U_L), the gas flux ($\rho_G U_G^S$) and the upstream pressure. The pressure field is defined in a staggered grid. U_b is the border velocity of the cells.

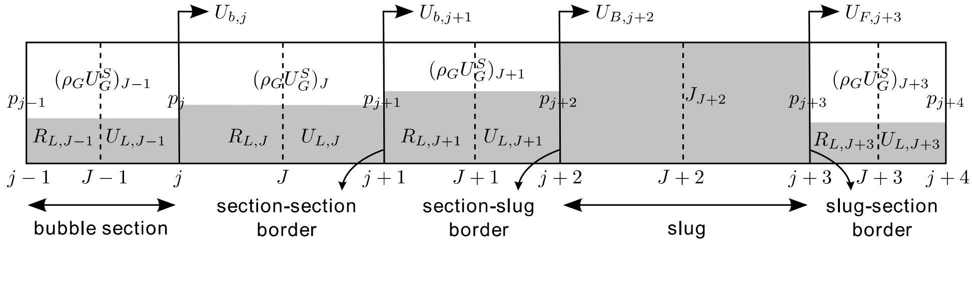

Figure 4. Computational grid

First Step: Pressure-Momentum Link

Considering gas mass conservation within a control volume *j*, the following expression can be derived:

$$\cancel{V}_{G,j}\frac{d\rho_{G,j}}{dt} = \frac{dm_{G,j}}{dt} - \rho_{G,j}\frac{d\cancel{V}_{G,j}}{dt} \tag{21}$$

where $\cancel{V}_{G,j} = 0.5\left(R_{G,J-1}L_{J-1} + R_{G,J}L_J\right)A$ is the gas volume in the cell *j* and *L* is the cell length.

Knowing that $d\rho_{G,j}/dt = (d\rho_{G,j}/dp_j).(dp_j/dt)$, one obtains:

$$p_j^{n+1} = \chi_j^n\left[\left(\rho_G U_G^S\right)_{J-1}^{n+1} - \left(\rho_G U_G^S\right)_J^{n+1}\right] + \psi_j^n \tag{22}$$

where

$$\chi_j^n = \frac{\delta t}{\dfrac{\cancel{V}_{G,j}^n}{A}\left[\dfrac{d\rho_G}{dp}\right]_j^n} \tag{23}$$

$$\psi_j^n = p_j^n + \frac{\delta t}{\dfrac{\cancel{V}_{G,j}^n}{A}\left[\dfrac{d\rho_G}{dp}\right]_j^n}\cdot\left(\rho_{G,j}\left(\left(R_L U_L\right)_{J-1}^n - \left(R_L U_L\right)_J^n\right) + R_{G,J-1}^n U_{b,J-1}^n\left(\rho_{G,j}^n - \rho_{G,J-1}^n\right) + R_{G,J}^n U_{b,J}^n\left(\rho_{G,J}^n - \rho_{G,j}^n\right)\right) \tag{24}$$

Equation (22) is used to calculate the pressure in all sections. However, there are two special regions where this equation must be replaced, namely the slug borders. Since the gas flux $(\rho_G U_G^S)_{J+2}$ in the slug is not known, the pressure p_{j+2} in the section-slug border is evaluated as a function of the mixture velocity J_{J+2}:

$$p_{j+2}^{n+1} = \chi_{j+2}^n\left[\left(\rho_G U_G^S\right)_{J+1}^{n+1} - \rho_{G,j+2}^n J_{J+2}^{n+1}\right] + \psi_{j+2}^n \tag{25}$$

$$\psi_{j+2}^n = p_{j+2}^n + \frac{\delta t}{\dfrac{\cancel{V}_{G,j+2}^n}{A}\left[\dfrac{d\rho_G}{dp}\right]_{j+2}^n}.\left(\rho_{G,j+2}\left(R_L U_L\right)_{J+1}^n + R_{G,J+1}^n U_{b,J+1}^n\left(\rho_{G,j+2}^n - \rho_{G,J+1}^n\right)\right) \tag{26}$$

Similarly, in the slug-section border the pressure p_{j+3} is given by:

$$p_{j+3}^{n+1} = \chi_{j+3}^n\left[\rho_{G,j+3}^n J_{J+2}^{n+1} - \left(\rho_G U_G^S\right)_{J+3}^{n+1}\right] + \psi_{j+3}^n \tag{27}$$

$$\psi_{j+3}^n = p_{j+3}^n + \frac{\delta t}{\dfrac{\cancel{V}_{G,j+3}^n}{A}\left[\dfrac{d\rho_G}{dp}\right]_{j+3}^n}\left(-\rho_{G,j+3}\left(R_L U_L\right)_{J+3}^n + R_{G,J+3}^n U_{b,J+3}^n\left(\rho_{G,J+3}^n - \rho_{G,j+3}^n\right)\right) \tag{28}$$

Gas Momentum Conservation. Considering the control volume *J* whose boundaries are located at *j* and *j+1* and replacing the pressures p_{j+1} and p_j through the Eq. (22), the gas momentum equation can be linearized with the finite difference method, yielding:

$$a_J^n\left(\rho_G U_G^S\right)_J^{n+1} = b_J^n\left(\rho_G U_G^S\right)_{J+1}^{n+1} + c_J^n\left(\rho_G U_G^S\right)_{J-1}^{n+1} + d_J^n \tag{29}$$

where

$$a_J^n = \frac{1}{\delta t} + b_J^n + c_J^n + \frac{1}{2}\left(\frac{S_G}{A_G}\lambda_G\left|U_G\right|\right)_J^n + \frac{1}{2}\left(\frac{S_i}{A_G}\lambda_i\left|U_G - U_L\right|\right)_J^n \tag{30}$$

$$b_J^n = -\frac{1}{L_J^n}\min\left(U_{G,j+1}^n - U_{b,j+1}^n, 0\right) + \frac{R_{G,J}^n}{L_J^n}\chi_{j+1}^n \tag{31}$$

$$c_J^n = \frac{1}{L_J^n}\max\left(U_{G,j}^n - U_{b,j}^n, 0\right) + \frac{R_{G,J}^n}{L_J^n}\chi_j^n \tag{32}$$

$$d_J^n = \frac{1}{\delta t}\left(\rho_G U_G^S\right)_J^n + \frac{R_{G,J}^n}{L_J^n}\left(\psi_j^n - \psi_{j+1}^n\right) + \frac{1}{2}\left(\frac{S_i}{A}\lambda_i\rho_G U_L^n\left|U_G - U_L\right|\right)_J^n \tag{33}$$

Equation (29) is used to calculate the gas flux in all sections. This equation is altered due to the pressure in the slug border whenever slugs are present in the flow.

In the section *J+1*, considering a control volume within the *j+1* and *j+2* boundaries, the gas momentum conservation becomes:

$$a_{J+1}^n\left(\rho_G U_G^S\right)_{J+1}^{n+1} = b_{J+1}^n J_{J+2}^{n+1} + c_{J+1}^n\left(\rho_G U_G^S\right)_J^{n+1} + d_{J+1}^n \tag{34}$$

where

$$a_{J+1}^n = \frac{1}{\delta t} + \frac{b_{J+1}^n}{\rho_{G,j+2}^n} + c_{J+1}^n + \frac{1}{2}\left(\frac{S_G}{A_G}\lambda_G\left|U_G\right|\right)_{J+1}^n + \frac{1}{2}\left(\frac{S_i}{A_G}\lambda_i\left|U_G - U_L\right|\right)_{J+1}^n \tag{35}$$

$$b_{J+1}^n = \rho_{G,j+2}^n\left[-\frac{1}{L_{J+1}^n}\min\left(U_{G,j+2}^n - U_{b,j+2}^n, 0\right) + \frac{R_{G,J+1}^n}{L_{J+1}^n}\chi_{j+2}^n\right] \tag{36}$$

$$c_{J+1}^n = \frac{1}{L_{J+1}^n}\max\left(U_{G,j+1}^n - U_{b,j+1}^n, 0\right) + \frac{R_{G,J+1}^n}{L_{J+1}^n}\chi_{j+1}^n \tag{37}$$

$$d_{J+1}^n = \begin{bmatrix} \frac{1}{\delta t}\left(\rho_G U_G^S\right)_{J+1}^n + \frac{R_{G,J+1}^n}{L_{J+1}^n}\left(\psi_{j+1}^n - \psi_{j+2}^n\right) + \frac{1}{2}\left(\frac{S_i}{A}\lambda_i\rho_G U_L^n\left|U_G - U_L\right|\right)_{J+1}^n \\ + \frac{\rho_{G,j+2}^n}{L_{J+1}^n}\min\left(U_{G,j+2}^n - U_{b,j+2}^n, 0\right)\left(R_L U_L\right)_{J+2}^n \end{bmatrix} \tag{38}$$

Likewise, in the section *J+3*, considering a control volume within the *j+3* e *j+4* boundaries, the gas momentum conservation becomes:

$$a_{J+3}^n\left(\rho_G U_G^S\right)_{J+3}^{n+1} = b_{J+3}^n\left(\rho_G U_G^S\right)_{J+4}^{n+1} + c_{J+3}^n J_{J+2}^{n+1} + d_{J+3}^n \tag{39}$$

where

$$a^n_{J+3} = \frac{1}{\delta t} + b^n_{J+3} + \frac{c^n_{J+3}}{\rho^n_{G,j+3}} + \frac{1}{2}\left(\frac{S_G}{A_G}\lambda_G|U_G|\right)^n_{J+3} + \frac{1}{2}\left(\frac{S_i}{A_G}\lambda_i|U_G - U_L|\right)^n_{J+3} \tag{40}$$

$$b^n_{J+3} = -\frac{1}{L^n_{J+3}}\min\left(U^n_{G,j+4} - U^n_{b,j+4}, 0\right) + \frac{R^n_{G,J+3}}{L^n_{J+3}}\chi^n_{j+4} \tag{41}$$

$$c^n_{J+3} = \rho^n_{G,j+3}\left[\frac{1}{L^n_{J+3}}\max\left(U^n_{G,j+3} - U^n_{b,j+3}, 0\right) + \frac{R^n_{G,J+3}}{L^n_{J+3}}\chi^n_{j+3}\right] \tag{42}$$

$$d^n_{J+3} = \left[\begin{array}{c} \frac{1}{\delta t}\left(\rho_G U^S_G\right)^n_{J+3} + \frac{R^n_{G,J+3}}{L^n_{J+3}}\left(\psi^n_{j+3} - \psi^n_{j+4}\right) + \frac{1}{2}\left(\frac{S_i}{A}\lambda_i\rho_G U^n_L|U_G - U_L|\right)^n_{J+3} \\ -\frac{\rho^n_{G,j+2}}{L^n_{J+3}}\max\left(U^n_{G,j+3} - U^n_{b,j+3}, 0\right)\left(R_L U_L\right)^n_{J+2} \end{array}\right] \tag{43}$$

Slug Momentum Conservation. Considering the control volume *J+2* whose boundaries are located at *j+2* e *j+3* the linearized liquid momentum conservation in the slug becomes:

$$a^n_{J+2}J^{n+1}_{J+2} = b^n_{J+2}\left(\rho_G U^S_G\right)^{n+1}_{J+3} + c^n_{J+2}\left(\rho_G U^S_G\right)^{n+1}_{J+1} + d^m_{J+2} \tag{44}$$

where

$$a^n_{J+2} = \rho_L\frac{L^n_{J+2}}{\delta t} + \rho_L\frac{R^n_{L,J+3}}{1 - R^n_{L,J+3}}\left(J^n_{J+2} - U^n_{L,J+1}\right) + \frac{\lambda_L\rho_L}{2D}L^n_{J+2}\left|J^n_{J+2}\right| + \rho^n_{G,j+3}\chi^n_{j+3} + \rho^n_{G,j+2}\chi^n_{j+2} \tag{45}$$

$$b^n_{J+2} = \chi^n_{j+3} \tag{46}$$

$$c^n_{J+2} = \chi^n_{j+2} \tag{47}$$

$$d^n_{J+2} = \psi^n_{j+2} - \psi^n_{j+3} - g\rho_L\left(h_{L,R} - h_{L,L}\right) + \rho_L\frac{L^n_{J+2}}{\delta t}J^n_{J+2} + \rho_L\frac{R^n_{L,J+3}}{1 - R^n_{L,J+3}}\left(J^n_{J+2} - U^n_{L,J+3}\right)U^n_{L,J+3} \tag{48}$$

In the above equations, $h_{L,L}$ and $h_{L,R}$ are the liquid levels to the left and to right of the slug, respectively.

To simplify the modelling of the fluid loss from the slug to the bubble, it was assumed in Eq. (44) that the amount of liquid mass picked up by the slug is the same it sheds $\left(U^n_B - J^n_{J+2} = U^n_F - J^n_{J+2}\right)$. During the liquid film solution (second step), the front and rear slug velocities are calculated and their border positions are updated through mass balances.

Second Step: Riemann Problem

To solve the liquid film momentum, the volumetric force term is zeroed, $F(R_L, U_L, U_G) = 0$, and its influence over the film is calculated during the first step, as explained later. Thus, Eq. (6) is rewritten as:

$$\frac{\partial}{\partial t}\left(R_L U_L\right) + \frac{\partial}{\partial x}\left(R_L U^2_L + \frac{1}{2}\kappa R^2_L\right) = 0 \tag{49}$$

Equations (5) and (49) have a weak solution since their characteristic curves may intersect. Therefore, the classical solution through the method of characteristics fails to provide multiple solutions or even a single one, whereas the weak solution may contain discontinuities.

In that case, the system of equations may be represented by the Riemann problem and has a weak solution between the left ($U_{l,L}$,$R_{l,L}$) and right ($U_{l,R}$,$R_{l,R}$) states. The solution will be either a shock wave or a rarefaction wave between the initial and the intermediate ($U_{l,M}$,$R_{l,M}$) states, according to the flow parameters. The variables $U_{l,L}$, $U_{l,R}$ and $U_{l,M}$ are the left, right and the intermediate state liquid velocity, respectively. The same is true for the volume fractions ($R_{l,L}$,$R_{l,R}$,$R_{l,M}$).

Table 3 presents the assumptions made for the different cases and that can be used to find the solution for the Riemann problem by solving Eq. (49).

In this work, the parameter κ has been assumed as constant for the calculations of the intermediate state between the sections, such that:

$$\kappa = \frac{\kappa_L L_L + \kappa_R L_R}{L_L + L_R} \tag{50}$$

where L_L is the cell length of the left state and L_R is the cell length of the right state.

Once the intermediate state is determined by the solution of the Riemann problem, the kind of solutions between the intermediate, the left and the right states and the border parameters between the sections can also be determined.

Table 3. Intermediate state determination

Left state - intermediate state solution	Shock wave $R_{l,M} > R_{l,L}$	$U_{l,M} = U_{l,L} - \sqrt{\frac{\kappa}{2}}\left(R_{l,M} - R_{l,L}\right)\sqrt{\frac{1}{R_{l,M}} + \frac{1}{R_{l,L}}}$
	Rarefaction wave $R_{l,M} < R_{l,L}$	$U_{l,M} = U_{l,L} - 2\sqrt{\kappa}\left(\sqrt{R_{l,M}} - \sqrt{R_{l,L}}\right)$
Right state - intermediate state solution	Shock wave $R_{l,M} > R_{l,R}$	$U_{l,M} = U_{l,R} + \sqrt{\frac{\kappa}{2}}\left(R_{l,M} - R_{l,R}\right)\sqrt{\frac{1}{R_{l,M}} + \frac{1}{R_{l,R}}}$
	Rarefaction wave $R_{l,M} < R_{l,R}$	$U_{l,M} = U_{l,R} + 2\sqrt{\kappa}\left(\sqrt{R_{l,M}} - \sqrt{R_{l,R}}\right)$

Figure 5 shows the calculation procedure after the intermediate states for a section become known. Using mass conservation, the so-called left and right intermediate states characterized by their volume fractions (R_{ML}, R_{MR}) and border velocities (U_{LL}, U_{RR}) can be found. Through the information given by those border velocities, the Courant-Friedrichs-Lewy (CFL) criterion is checked to verify whether the displacement of the left solution does not override the displacement of the right solution for the given time step in a same section. If the criterion is violated, the CFL-breaching section is merged with the neighbouring section of closest holdup and the calculation procedure explained above is repeated for this newly merged section.

For each section, the right intermediate state between the previous and the current sections, and the left intermediate state between the current and the posterior sections can be determined. Then, the volume fraction and the liquid velocity as well as the border displacements are updated. The calculations of these variables are done by using weighted averages:

$$x_j^{n+1} = x_j^n + U_{b,j}\delta t \qquad x_{RR,j}^{n+1} = x_j^n + U_{RR,j}\delta t \tag{51}$$

$$x_{j+1}^{n+1} = x_{j+1}^n + U_{b,j+1}\delta t \qquad x_{LL,j+1}^{n+1} = x_{j+1}^n + U_{LL,j+1}\delta t \tag{52}$$

$$R_{l,J}^{n+1} = \frac{R_{l,J}^n\left(x_{LL,j+1}^{n+1} - x_{RR,j}^{n+1}\right) + R_{ML,j+1}^n\left(x_{j+1}^{n+1} - x_{LL,j+1}^{n+1}\right) + R_{MR,j}^n\left(x_{RR,j}^{n+1} - x_j^{n+1}\right)}{x_{j+1}^{n+1} - x_j^{n+1}} \tag{53}$$

$$U_{l,J}^{n+1} = \frac{R_{l,J}^n U_{l,J}^n\left(x_{LL,j+1}^{n+1} - x_{RR,j}^{n+1}\right) + R_{ML,j+1}^n U_{ML,j+1}^n\left(x_{j+1}^{n+1} - x_{LL,j+1}^{n+1}\right) + R_{MR,j}^n U_{MR,j}^n\left(x_{RR,j}^{n+1} - x_j^{n+1}\right)}{\left(x_{j+1}^{n+1} - x_j^{n+1}\right)R_{l,J}^{n+1}} \tag{54}$$

Velocities are assigned to the borders of the intermediate states (U_{LL}, U_{RR}) during the solution of the liquid film, meaning that the velocity of the section border velocity (U_b) must be chosen. In order to follow the shock waves, Renault proposed $U_b = U_{RR}$ should a wave shock on the right exists. Otherwise, the border velocity is equal to the liquid velocity of the intermediate state ($U_b = U_{l,M}$). This way, the smooth profile of the bubble nose and the hydraulic jump that occurs in the slug front may be modelled in a more realistic manner.

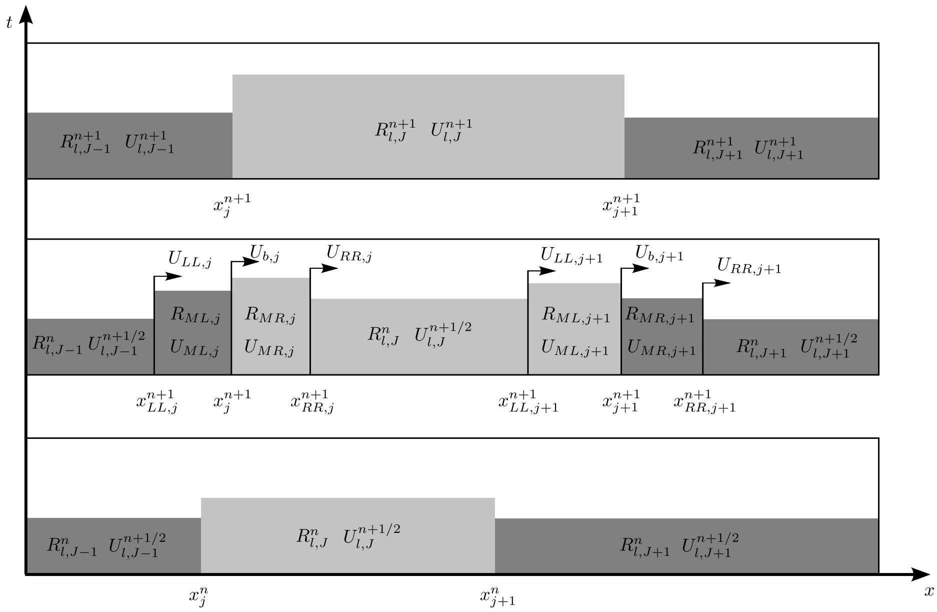

Figure 5. Liquid film solution

Nine different situations may occur: the four classical cases (rarefaction-rarefaction, shock-shock, shock-rarefaction, rarefaction-shock); the saturated shock ($R_{l,M} > 1$); rarefaction-rarefaction with the formation of a dry bed ($R_{l,M} \leq 0$); left rarefaction with a dry bed in the right ($R_{l,R} = 0$); a dry bed in the left with right rarefaction ($R_{l,L} = 0$) and the section-slug case where the border velocity is calculated by means of the bubble translational velocity. More details on the calculations for all those cases are found in Conte (2014) and Renault (2007).

Boundary Condition and Initial Condition

Pipe inlet is modelled as a cell whose liquid and gas superficial velocities are known. Therefore, the volume fraction and pressure are not given and must be evaluated so that they can be used as boundary conditions in the system solution for the first step. Linear extrapolations based on the neighbouring cells can be used, but during the simulations (especially at their beginning) some pressure fluctuations due to numerical effects have been observed. This is because the guessed values calculated by the linear extrapolation are based on old values, and that is not adequate for intermittent flow computations.

The system of equations is then solved iteratively until both the gas flux, used as a boundary condition, and the pressure converge through the secant method. In the second step, the volume fraction and the velocity of the inlet cell are calculated as it is done in any other section of the flow.

The pipe outlet cell is considered as a separator at constant pressure. The cells are cut off as they come out and finally excluded when they exit the pipe completely. The outlet cell pressure is a boundary condition to the tridiagonal system and the liquid flux in this cell is null, $R_{L,out} = 0$, as if the liquid mass vanishes upon exiting the pipe, as shown in Fig. 6. The gas flux is assumed to be equal to the previous cell or null, if there is a slug leaving the pipe.

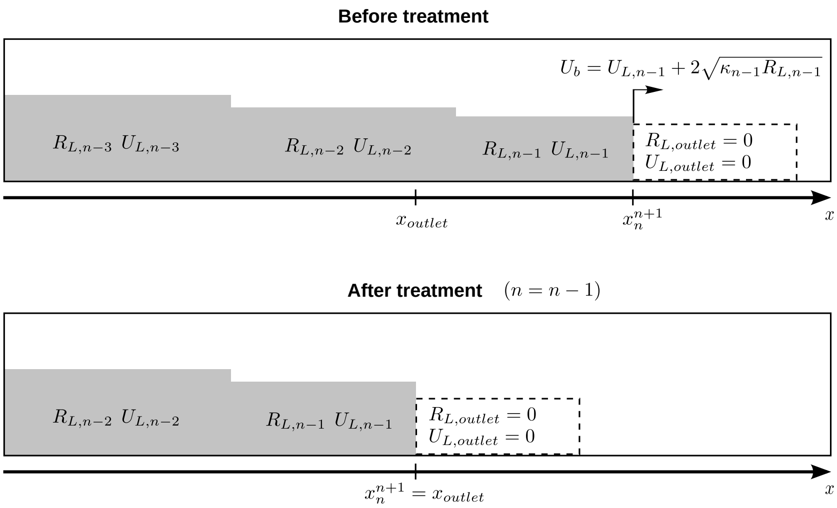

Figure 6. Pipe outlet

Stratified smooth flow in steady state condition is assumed at the start of the calculations, so that the volumetric forces are null $F(R_L, U_L, U_G) = 0$. This allows obtaining the volume fraction for this condition for given superficial velocities. After the simulation has started, the flow is free to develop itself.

The boundary conditions are the liquid and gas superficial velocities (U_L^S, U_L^S) at the inlet and the pressure at the outlet, which is usually considered as being equal to the atmospheric pressure ($p_{out} = p_{atm}$).

Gas mass correction and solution details

The gas mass inside the bubbles must be corrected whenever there are slugs in the flow. When the initial gas mass in the bubble is known, the following relation is applied to ensure gas mass conservation:

$$corr = \frac{m_G^0 - m_G^n}{\mathcal{V}_G^0}\left[\frac{\partial \rho_G}{\partial p}\right]^{-1} \tag{55}$$

where m_G^0 and $\forall_G^0$ are the initial mass and volume of the gas in the bubble, respectively, and m_G^n is the current gas mass. This correction is applied to the coefficient ψ_J^n of Eq. (24) and it is equally split for each section that makes up the bubble.

The influence over the liquid of the volumetric force F, Eq. (7), is evaluated at the end of the first block, as presented below. The term F was modified to include the partial derivative with respect to U_L (Renault, 2007):

$$F\left(R_L,U_L,U_G\right)=F\left(R_L,\bar{U}_L,U_G\right)+dU_L\left(\frac{\partial F}{\partial U_L}\right)_{R_L,U_G} \tag{56}$$

Thus, the influence of the volumetric forces is calculated as:

$$U_{L,J}^{n+1/2}=\frac{\left[U_{L,J}^{n}+\dfrac{\delta t}{\rho_L}F\left(R_{L,J}^{n},U_{L,J}^{n},U_{G,J}^{n+1}\right)-U_{L,J}^{n}\dfrac{\delta t}{\rho_L}\dfrac{\partial F}{\partial U_L}\left(R_{L,J}^{n},U_{L,J}^{n},U_{G,J}^{n+1}\right)\right]}{1-\dfrac{\delta t}{\rho_L}\dfrac{\partial F}{\partial U_L}\left(R_{L,J}^{n},U_{L,J}^{n},U_{G,J}^{n+1}\right)} \tag{57}$$

Due to the lagrangian characteristic of the model, the sections may grow during the simulations. After having the cell displacements determined, the sections that exceeded a critical value ($L_J > L_{crit}$) are split so as to keep the spatial accuracy. Those that achieve a volume fraction equal or bigger than $R_L \geq R_{L,crit} = 0.98$ become slugs and the missing volume required to reach $R_L = 1$ is taken from the neighbouring sections.

Algorithm

The discretization model was implemented with Intel® Visual Fortran. The program execution is composed by three main blocks:

- 1st block:
  1) Eq. (55) is applied to the gas bubbles in the pipe;
  2) Eqs. (29) and (44), which form a tridiagonal system $a_J^n X_J^{n+1}=b_J^n X_{J+1}^{n+1}+c_J^n X_{J-1}^{n+1}+d_J^n$, are solved using the TDMA method for the gas flux in the sections and for the mixture velocity in the slugs;
  3) Eq. (22) is solved for the pressure;
  4) If the inlet gas flux has not converged, go to step 2;
  5) Eq. (57) is solved for every section.

- 2nd block:
  1) The Riemann problem is solved for every section border using equations in Tab. 3;
  2) The CFL criterion is checked for every section;
  3) Eqs. (51), (52), (53) and (54) are solved for the section position, velocity of the liquid film and section holdup;
  4) The slug front position is updated.

- 3th block:
  1) If $R_L \geq R_{L,crit}$ the section becomes a slug;
  2) Exclude sections or slug portions that have exited the pipe;
  3) Split sections with $L_J > L_{crit}$.

4 NUMERICAL RESULTS

Simulations were carried out with the same configurations of the experimental data obtained in NUEM/UTFPR and presented in Tab. 4. The fluids were water and air at ambient pressure. The flow developed in a 2-section pipe with different inclinations: the first one with -3º (downward flow) and the second one horizontal. This geometry was chosen so as to eliminate the influence of the mixer in the pipe inlet and to ensure the onset of slug flow from a stratified flow, according to the Kelvin- Helmholtz mechanism. The critical length and the gas compressibility used were, respectively, $L_{crit}=2\delta x$ and $\partial\rho_G/\partial p=1.1\ 10^{-5}\ kg/m^3Pa$. Figure 7 shows the location of the virtual probes along the pipe with the corresponding measurement stations.

Table 4. Geometrical configurations

Pipe length [m]	8.768 (337.2D)
Downward pipe lenght [m]	2.720 (104.6D)
Horizontal pipe lenght [m]	6.048 (232.6D)
Pipe diameter [m]	0.026
Liquid density [kg/m³]	1000
Liquid viscosity [Pa.s]	8.55E-4
Location of probe #1 [m]	2.953 (113.6D)
Location of probe #2 [m]	4.020 (154.6D)
Location of probe #3 [m]	5.285 (203.3D)
Location of probe #4 [m]	5.970 (229.6D)
Location of probe #5 [m]	6.778 (260.7D)
Location of probe #6 [m]	8.700 (334.6D)

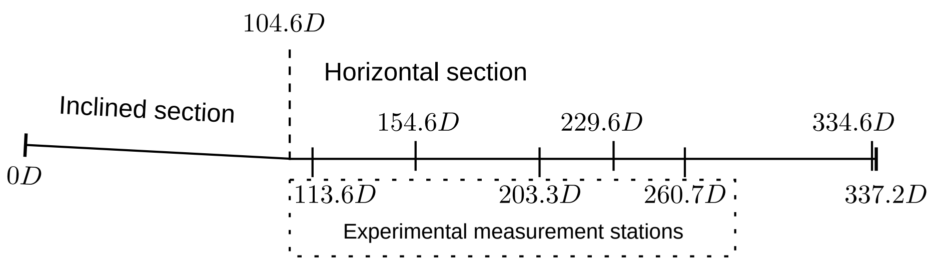

Figure 7. Location of the virtual probes

The experiments were performed for three pairs of liquid and gas superficial velocities. As Fig. 8(a) shows, all pairs are below the stratified-slug flow transition curve for the first section condition (downward flow). In Fig. 8(b) every point is above the VKH curve. However, the first pair is above the IKH curve (in a transition region for the model), the second one is above the IKH curve (ill-posed region) and the last point is below the IKH curve (well-posed region).

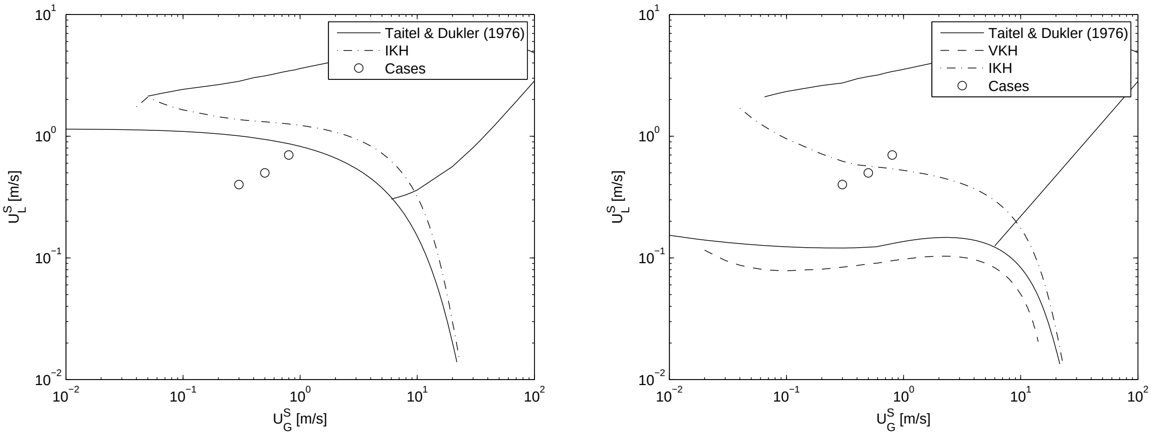

Figure 8. Experimental flow rate pairs location in the flow map for (a) -3° inclination (b) 0°

Since the three pairs are below the VKH curve in the inclined section (not visible because the VKH curve coincides with the stratified-slug flow transition), the numerical flow will be always stratified in the downward section and disturbances can grow until the formation of slug flow in the horizontal section as it occurs with the actual flow. Parameter κ is constrained to a minimum value in order to avoid numerical issues in the ill-posed cases.

Figure 9 shows a snapshot of the simulation for U_L^S=0.50 *m/s* and U_G^S=0.50 *m/s* after 8.9 seconds of flow. The vertical dashed line represents the elbow. Analyzing this figure, it can be noted that the flow remained stratified in the inclined section and changes to slug flow in the horizontal section.

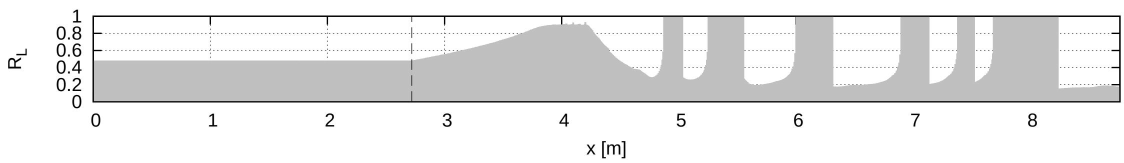

Figure 9. Snapshot of the simulations

The influence of the integration parameters was verified for U_L^S=0.50 *m/s* e U_G^S=0.50 *m/s*. Different time steps and average section lengths were tested to evaluate the slug frequency (i.e. number of slugs per unit time) in the probe #6, as Tab. 5 shows.

Table 5. Slug frequency in the probe #6

δt \ δx	0.020	0.010	0.005	0.001
0.010	1.07	1.35	1.40	0.214
0.005	1.06	1.53	2.11	0.748
0.001	1.02	1.46	1.83	4.33

Tab. 5 shows that the integration parameters are highly relevant to the slug initiation. The slug frequency decrease observed when the grid is highly refined can be explained after an analysis of the CFL criterion, which is calculated by the inequality:

$$(U_{RR,j} - U_{LL,j+1})\delta t < L_j \tag{58}$$

The velocities found during the flow development are independent of the integration parameters. Therefore, keeping the same time step and refining the computation grid results in an increased sensibility of the CFL criterion. Thus, small perturbations that would enable a wave formation are eliminated during the simulation, decreasing the slug frequency. Based on this behaviour it was proposed that the minimum grid length for a given time step is calculated as:

$$\delta x > U_L \delta t \tag{59}$$

This inequality indicates the range for which the slug generation is affected by the CFL criterion. To prove its validity, three flow rate pairs were simulated for various grid lengths at a fixed time step equal to δt=0.01s. Figure 10 presents the slug frequencies obtained according to δx. Vertical lines represent the criterion given by Eq. (59). It is observed that the proposed relation can predict the region where frequency decreases considerably due to the CFL criterion implemented in the code.

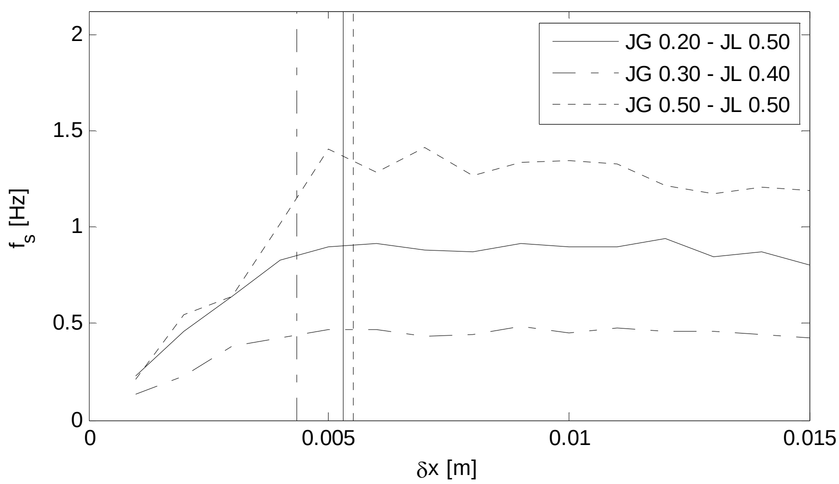

Figure 10. Verification of the proposed criterion for minimum grid length

The main slug flow-related parameters experimentally measured at NUEM/UTFPR will be compared with the variables obtained numerically so that the reliability of the model presented in this work can be evaluated. The slug frequency, unit-cell frequency (inverse of a unit-cell period), bubble length and slug length are those parameters. The integration parameters used are shown in Tab. 6.

Table 6. Integration parameters

Point	U_G^S	U_L^S	δt	δx	δx_{min}
#1	0.5	0.5	0.005	0.005	0.003
#2	0.8	0.7	0.005	0.020	0.004
#3	0.3	0.4	0.005	0.005	0.002

Numerical results of point #1, which lies in the transition between the well-posed and the ill-posed region, showed good agreement with the experimental data, as shown in Fig.11. The same can be observed for the point #2, although the model is located inside the ill-posed region.

For the point #3, located in the well-posed region, the numerical slug flow generation was smaller than that observed experimentally. This can be observed in the distribution of the numerical unit-cell frequency, which is shifted to the left compared to the experimental, and by the presence of longer slugs and bubbles in the simulations.

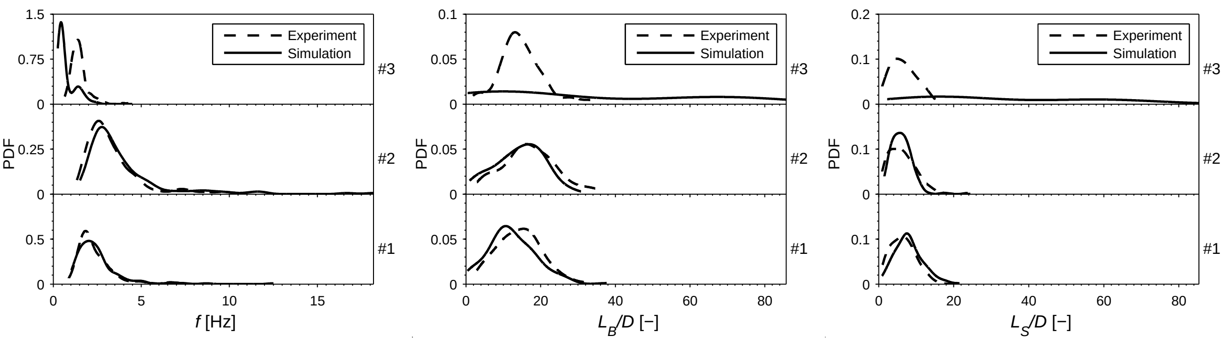

Figure 11. Probability density function for (a) unit-cell frequency (b) bubble length (c) slug length

Table 7 shows the experimental and numerical slug frequency at the last measurement station and at probe #5, respectively, and the relative error between these frequencies. As expected, the frequency numerically calculated in point #3 is smaller than the experimental. On the other hand, the errors for the points #1 and #2 were low.

Table 7. Experimental and numerical results for the slug frequency

Point	U_G^S	U_L^S	$\overline{f}_{S,EXP}$	$\overline{f}_{S,SIM}$	$Error = \dfrac{\overline{f}_{S,EXP} - \overline{f}_{S,SIM}}{\overline{f}_{S,EXP}}$
#1	0.5	0.5	2.09	2.12	1.3 %
#2	0.8	0.7	2.88	3.21	11 %
#3	0.3	0.4	1.38	0.527	62 %

This reflects a model feature: for the points in or near the “theoretically” ill-posed region the model has a great ability to generate slug flow and its results show good agreement with the experimental data. On the other hand, the farther the pair is from the “theoretically” ill-posed region the more the slug flow generation rate reduces, even more than the experimental, resulting in the separation of numerical and experimental data.

CONCLUSIONS

A model from the literature aimed at capturing slugs for horizontal two-phase flows was analyzed. The model is based on the two-fluid model and it is capable of tracking down waves that arise in the gas-liquid interface and slugs possibly generated by them. Three cases were simulated: in the inclined section, all cases in the stratified flow region; in the horizontal section, two cases below the IKH curve and one above the IKH curve where the model is mathematically ill-posed. The numerical results were compared with experimental data acquired at NUEM/UTFPR.

Some conclusions from the results and discussions outlined throughout this work are highlighted below:

i) The model was capable to simulate the correct slug flow profile as showed in Fig. 9. The downward flow kept a stratified profile. The liquid film height increased after the elbow allowing slugs to emerge and to establish slug flow in the horizontal section, as expected by the analysis of Fig. 8. The same behaviour was observed in the test facility during the acquisition of the experimental data.

ii) Integration parameters influenced the slug frequency calculations. A criterion based on the CFL criterion for the minimum grid length in order to maximize the number of slugs in the simulations for a given time step was proposed. The aforementioned criterion was tested and proved to be valid, as shown in Fig. 10.

iii) Considering the complexity of the problem, the model reproduced the experimental data with good accuracy, except for case #3 in which the slug frequency was considerably smaller than the experimental values. This unexpected behaviour suggests that the model seems to be more effective in the region close to the IKH curve. Moreover, the ability of the model in capturing slugs seems to decrease more than the expected according to the experimental data.

Further studies and more experiments are needed. Also, model parameters like friction factors and the wake effect coefficient should be tested. An investigation on the influence of the parameter κ and simulations for the stratified-to-slug flow transition zone are also suggested.

ACKNOWLEDGEMENTS

The authors wish to express their gratitude for all the technical and financial support provided by the TE/CENPES/PETROBRAS.

REFERENCES

Barnea, D., Taitel Y., 1993. A model for slug length distribution in gas-liquid slug flow. Int. J. Multiphase Flow, 19, 829-838.

Bendiksen, K.H., Malnes, D., Moe, R., Nuland, S., 1991. The dynamic two-fluid model OLGA: Theory and application. SPE Production Engineering, May 1991, 171-180.

Biberg, D., 2005. Mathematical models for two-phase stratified pipe flow. Ph.D Thesis. University of Oslo.

Brill, J. P., Schmidt, Z., Coberly, W.A., Herring, J.D., Moore, D.W., Analysis of Two-Phase Tests in Large-Diameter Flow Lines in Prudhoe Bay Field. Soc. Petr. Eng. J. 271, p. 363-78, 1981.

Cohen, S.L., Hanratty, T.J. 1968. Effects of waves at a gas-liquid interface on a turbulent air flow. J. Fluid Mech. 31, 217-226.

Conte, M.G. Numerical and experimental study of slug initiation for gas-liquid two-phase-flows. 2014. 133p. Dissertação (Mestrado em Engenharia) - Programa de Pós-graduação em Engenharia Mecânica e de Materiais, Universidade Tecnológica Federal do Paraná, Curitiba, 2014.

Dukler, A.E. and Hubbard, M.G., 1975. "A Model for Gas-Liquid Slug Flow in Horizontal and Near Horizontal Tubes", Ind. Eng. Chem. Fundam., Vol. 14, pp. 337-345.

Fan, Z., Lusseyran, F., Hanratty, T.J., Initiation of slugs in horizontal gas-liquid flows. AIChE Journal, November 1993.

Fernandes, R.C., Semiat, R. and Dukler, A.E., 1983. Hydrodynamic Model for Gas-Liquid Slug Flow in Vertical Tubes. AIChE Journal, vol. 29(6), pp. 981-989.

Ishii, M. 1975. "Thermo-fluid dynamic theory of two-phase flow" Collection de la Direction des Etudes et Recherches d'Electricite de France, no. 22, Eyrolles, Paris, France.

Issa, R.I., Kempf, M.H.W., 2003. Simulation of slug flow in horizontal or nearly horizontal pipes with the two-fluid model. Int. J. Multiphase Flow 29, 69—95.

Kjeldby, T.K., Henkes, R.A.W.M., Nydal, O.J., 2013. Lagrangian slug flow modeling and sensitivity on hydrodynamic slug initiation methods in a severe slugging case. Int. J. Multiphase Flow 53, 29-39.

Lin, P.Y. and Hanratty, T.J., Prediction of the initiation of slugs with linear stability theory. Int. J. Multiphase Flow, Vol. 12, No. 1, pp. 79-98, 1986.

Nydal, O.J., Pintus, S., Andreussi, P., Statistical characterization of slug flow in horizontal pipes. Int. J. Multiphase Flow, Vol. 18, No. 3, pp. 439-453, 1992.

Renault, F. 2007. A Lagrangian slug capturing scheme for gas-liquid flows in pipes. Norwegian University of Science and Technology Faculty of Engineering Science and Technology Department of Energy and Process Engineering. (PhD Thesis).

Rodrigues, H.T., Morales, R.E.M., Mazza, R.A., Rosa, E.S. 2008. Horizontal slug flow properties captured by intermittent slug tracking model. 12th Brazilian Congress of Thermal Engineering and Sciences, November 10-14, Belo Horizonte, MG.

Taitel, Y., Barnea, D. 1990. "Two phase slug flow", In Advances in Heat Transfer (editted by Harnett, J.P. and Irvine, T.F. Jr), v. 20, pp. 83-132.

Taitel, Y., Dukler, A.E., 1976. A model for predicting flow regime transitions in horizontal and near horizontal gasliquid flow. AIChE J 22, 47-55.

Scott, S. and Kouba, G.: "Advances in Slug Flow Characterization for Horizontal and Slightly Inclined Pipelines," SPE Production and Facilities J. (1990).

van Hout, R., Barnea, D., Shemer, L., Evolution of statistical parameters of gas-liquid slug flow along vertical pipes. Int. J. Multiphase Flow 27, 1579-1602, 2001.

Wallis, G.B., 1969. One-dimensional two-phase flow. McGraw-Hill.

Woods, B.D., Fan, Z., Hanratty, T.J., Frequency and development of slugs in a horizontal pipe at large liquid flows. Int. J. Multiphase Flow 32, 902-925, 2006.

Zheng, G., Brill, J.P., Tailel, Y., Slug flow behavior in a hilly terrain pipeline. Int. J. Multiphase Flow, Vol. 20, No. 1, pp. 63-79, 1994.